Experimental Thermal and Fluid Science 110 (2020) 109941

Contents lists available at ScienceDirect

Experimental Thermal and Fluid Science

journal homepage: www.elsevier.com/locate/etfs

Experimental study of particulate fouling in partially filled channel with open-cell metal foam

F. Shikh Anuar[a,*], Kamel Hooman[b], M.R. Malayeri[c,d], Iman Ashtiani Abdi[e]

[a] Centre for Advanced Research on Energy, Universiti Teknikal Malaysia Melaka, Durian Tunggal, Melaka, Malaysia
[b] School of Mechanical and Mining Engineering, The University of Queensland, Queensland, Australia
[c] School of Chemical and Petroleum Engineering, Shiraz University, Shiraz, Iran
[d] Institut für Verfahrenstechnik und Umwelttechnik, Technical University of Dresden, Dresden, Germany
[e] Queensland University of Technology, Brisbane City, Queensland, Australia

ARTICLE INFO

Keywords:
Heat exchanger fouling
Particle deposition
Partially filled channel
Metal foam
Pressure drop

ABSTRACT

This study experimentally investigates particle transport and deposition processes in a partially filled channel with an open-cell metal foam. Various blockage ratio (a ratio of foam height and channel height) in range of 0.05–0.39, and pore density (10 and 30 PPI) were used to determine the effects of the foam microstructure and exterior shape on the propensity of particulate fouling. In-situ observations were conducted using a high-speed camera to determine the particle trajectory and velocity in the partially filled channel. Result shows a complex transport and deposition process, which is significantly influenced by the particle size and pore diameter. If merely considering the exterior shape of the foam, a higher blockage ratio causes more deposition in the upstream region. While, a low blockage ratio causes more deposition on the top surface of the foam block, regardless of pore density. These results demonstrate that the foam arrangement and heights play primary roles in influencing the preferential deposition areas, which is originally associated with flow behaviours in the partially filled channel. Interestingly, the foam microstructure not only blocks and traps the flowing particles, yet causing the breakage of particle clusters. These particles either disperse within the incoming flow or cause more depositions on the foam surfaces. The build-up deposits would increase the pressure drops, as expected, but the effects of pore density become insignificant over time.

1. Introduction

Open-cell metal foams are highly porous materials consist of interconnected ligaments and randomly distributed voids. The ligaments made of highly conductive materials (e.g., aluminium or copper) allow conduction heat transfer, while interfacial convection happens when the fluid flows pass through the voids or pores. By offering different modes of heat transfer, the open-cell metal foams show a tendency to overwhelm the existing heat exchanger thermal performances. They have been studied as a potential replacement to various heat exchangers in the industries such as exhaust gas recirculation (EGR) cooler [1], tube-in-tube counter-flow heat exchanger [2], inserts of tube heat exchanger [3] and annulus [4]. Many studies [5,6] have discussed the excellent thermal performance of open-cell metal foam heat exchanger under a clean environment, which is attributed to its high thermal conductivity material and complex pore-ligament construction that provide large heat transfer area per unit of volume and excellent flow mixing.

Alternatively, the metal foam microstructures that offer tortuous flow path [6] and acting as turbulence promoters [7] might be able to (i) reduce fouling from particle re-entrainment or (ii) increase fouling rates from turbulence impactions. To explore these possibilities, the metal foam performances are investigated further under a fouled condition such as exhaust gas recirculation system [1,8], and air-cooled heat exchanger [9–11]. Until recently (2018), most of the published literature on the fouling of metal foam were performed numerically [9,11–13] and analytically [7,14]. While, the existing experimental studies [8,15,16] focused on pressure drop effects, thermal effectiveness and thermal resistances. There is also an attempt to understand fluid-particle physics and the propensity of fouling for the complicated foam microstructures by applying an idealized porous media [17]. However, to the best authors' knowledge, this is no published literature of particle deposition and fouling processes using a real open-cell metal foam. Due to its complicated structure, a thorough experimental study

* Corresponding author.
E-mail address: fadhilah@utem.edu.my (F. Shikh Anuar).

https://doi.org/10.1016/j.expthermflusci.2019.109941
Received 25 January 2019; Received in revised form 23 September 2019; Accepted 25 September 2019
Available online 26 September 2019
0894-1777/

Nomenclature

D	diameter (m)
D50	50% of the particles in the sample > $\overline{d_p}$
$\overline{d_p}$	average particle diameter (m)
f#	lens f-number
FOV	field of view
fps	frame per seconds
h	foam height (m)
H	channel height (m)
h/H	blockage ratio
k	thermal conductivity (W/m·K)
L	pressure taps distance (m)
Lf	foam length (m); Lf = 0 = leading edge
lpm	litre per min
N	number of sample size
ΔP	pressure drop (Pa)
PPI	pore per inch
Re	Reynolds number
ROI	region of interest
t	recording duration (s)
u	velocity (m/s)
u_o	inlet velocity (m/s)
$\overline{u}$	average velocity (m/s)
wf	foam width (m)
x	streamwise position (m)
X	FOV streamwise length (m)
y	transversal position (m)
Y	FOV transversal length (m)

Subscripts

p	particle
Dh	hydraulic diameter (m)

Greek symbols

ε	porosity
ρ	density (kg/m^3)

is required to understand the underlying mechanisms of fouling in details.

Muley et al. [1] in their study on the metal foam as an alternative to a conventional wavy plate-fin heat exchanger in the EGR application found that the foam could have better thermal effectiveness but at the expenses of high pressure drop. The authors also suggested for further investigations under a fouled condition, as the inherent random cell structures of the metal foam may susceptible to fouling. However, Hooman and Malayeri [8] positively argued that an appropriate foam design could achieve a superior thermal performance at a reasonable pressure drop as compared to no-foam cases. They found that the low pore density foam; 20 PPI would have a higher pressure drop than 40 PPI foam, before reaching a similar value after four hours soot injection. While, a thicker foam (foam height, h = 4 mm) showed a higher pressure drop than 3 mm foam after two hours exposure. Besides, they found the heat transfer of the same PPI foams with different heights remain the same, but the 20 PPI foam would perform better than 40 PPI foam. Odabaee et al. [9] used ANSYS software to model a uniform deposition layer on a metal foam-wrapped tube bundle. Their result shows that the pressure drops of the fouled metal foam would increase up to 44% as compared to its clean condition even with only 0.01 mm deposition thickness. However, the remarkable increments of thermal resistances were seen only with a higher deposition thickness, e.g., 0.1 and 0.2 mm, regardless of inlet velocity from 1 to 7 m/s. Hooman et al. [7] considered a cubic cell model in investigating the effects of particle deposition in a metal foam heat exchanger. Their result shows that the pressure drop of a fouled metal foam increased up to three-order magnitude higher than its clean condition, evidently with the high pore density foam. The authors [7,9] stated that the dominant mechanisms in their studies are the gravitational force and inertial impaction because of the large particle size (10–400 μm) and the existence of ligament restrictions. It is also worthy to note that even though their studies assumed a uniform distribution of particle deposition, they have also suggested a requirement for further investigations as the nature of the metal foam itself may impose continuous changes of pressure, velocity and temperature profiles.

Like Odabaee et al. [9], Sauret et al. [10] also numerically studied the particle deposition on a single-row metal foam-wrapped tube bundle based on the same geometry of a real metal foam [18]. However, Sauret et al. [10] injected 5000 soot particles ($\rho = 2000\ kg/m^3$, $10\ \mu m \leq d_p \leq 250\ \mu m$) rather than assuming a uniform particle deposition. The authors applied a Lagrangian particle-tracking model and considered the possibilities for the particles to rebound and stick to the tube wall. The result shows that the heat transfer coefficient decreases with the increase of pore density (5–50 PPI), but showing different values at the front tube (up to 15 W/m^2 K) and rear region (3.0 W/m^2 K). Consequently, a higher deposition and particle volume fraction were observed at the front tube as compared to the rear region. Also, a large recirculation zone and weak backward velocity at the rear region are also additional factors that cause difficulty in carrying the particles back to the rear wall. Sauret et al. [13] extended their study [10] by investigating the effects of different particle size distribution and preferential particle deposition area in the same foam configuration. Similarly, more particles deposit in the front region and only small particles ($d_p < 20\ \mu m$) deposited in the rear regions. They also found most of the particles trapped within the porous structure, rather than moving towards the tube wall.

It is worthy to mention that Kuruneru et al. [11,19–21] have reported most of the fouling studies on the metal foam heat exchangers. However, their works mostly involved numerical approaches or experiments with idealized metal foams. The proposed idealized metal foams were made of an arrangement of several cylinder and square shape to mimic porous channel. Unfortunately, these idealized foams are not representing the real complexity of the foam microstructure. However, this approach is more feasible, considering the possibility of structure damage due to the deposited particles and high cost specimens for repeating experiments. For example, Kuruneru et al. [19] investigated 500 μm wood-dust deposition in five idealized porous channel configurations with different porosities, ε from 72 to 93%. Their result shows that the deposition could be increased by decreasing the porosity. They also found a higher particle deposition at the leading edge of obstacles (idealized ligaments) than the trailing edge. They stated that the inertial impaction is more profound at the leading edge as compared to the gravitational effects. Also, their numerical result of velocity vector using ANSYS Fluent agrees with the preferential deposition areas in the experiment. In another study, Kuruneru et al. [20] used OpenFOAM software and soft-sphere discrete element method to study the transport mechanisms of the sandstone and sawdust ($\overline{d_p} = 35 \pm 10\ \mu m$) in circular obstructions ($\varepsilon = 0.9$). The sandstone particles show a higher deposition fraction and pressure drop, while the sawdust deposition is insignificant and could be neglected. Their numerical pressure drop shows a good agreement with a modified Darcy equation. The inertia and gravitational sedimentation are the dominant mechanisms for the high density particle; sandstone, while particle interception is more profound with the sawdust because of its lower inertia.

Kuruneru et al. [21] used a finite volume method and discrete element method (FVM-DEM) to study fouling on an array of a circular cylinder. They assumed a laminar and isothermal condition, where only drag and gravitational forces were considered as the transport mechanisms for 50 and 70 μm particles. The result shows no deposition for the smaller particles, regardless of the injection rate, while the larger particles tend to clog the pores. A higher injection rate causes more clogging within the porous structure, particularly for 70 μm, which results in a lower porosity than 50 μm. The findings show that the deposition fraction and pressure drop increase linearly, and they justified the variation of data over time due to fouling layer thickness and surface area of the particle itself. Using idealized Weaire-Phelan metal foam geometry, Kuruneru et al. [11] attempted to model a real metal foam. The findings show only the pressure drop at low inlet velocity ($u_o < 1.0$ m/s) is successfully modelled through this method. They also assured that regardless of different porosities (ε = 0.95 and 0.98) and ligament thickness (0.09 and 0.17 mm), the foam microstructures are always susceptible to fouling.

Due to its complex pore-ligament construction, there is disagreement about using this kind of heat exchanger under a fouled condition [1,8]. However, the feasibility of open-cell metal foam heat exchanger with particle-laden flows must be examined thoroughly, especially due to the existence of secondary and mixing flows in the partially filled channel with open-cell metal foam [22]. These mixing flows at the interface and inside the porous structure may cause particle detachment and lesser deposits within its structure. Therefore, understanding the underlying mechanisms of the fouling in the porous structure is important to come out with a proper foam design. This experimental study aims to shed light on the particle transport and deposition processes in a partially filled channel with metal foam through in-situ observations. This includes the determination of particle preferential deposition area in that configuration. The fouling effects on the pressure drop performance are also determined. This study focuses on the influence of foam itself, while the other contributing factors, e.g., inlet velocity, temperature gradient, and particle injection rate are kept constant.

2. Experimental setup

2.1. Test rig and measurements

A series of experiments were performed in a small blown-type wind tunnel, consists of (1) blower, (2) heater, (3) particle injector (4) test section (5) filter and (6) flexible exhaust duct as shown schematically in Fig. 1. The ambient air was sucked through the blower, to pass through the heater and the settling chamber before entering the test section. The test section size is 0.078 m (H) × 0.10 m (W) × 0.35 m (L_c), which is partially filled with an open-cell metal foam block (Fig. 2). The test section walls are made of transparent glass (Quartz) that provide optical access to the flow. The inlet air velocity is set to 6.2 m/s by downsizing the size of the inlet tube using a gauge valve [23] with the Reynolds number (Re_{Dh}) of an empty channel is 36,000. Accordingly, the experiments were conducted in a turbulent flow. The details of the wind tunnel can be found in [24]. A fouled condition was created by injecting solid particles (see Section 2.2) at 1.67×10^{-5} kg/s using a vibratory feeder (Fritsch – Laborette 24). To make sure the particle can be dispersed uniformly across the partially filled section, the particle injector is positioned about 1.0 m far away from the test section, right before the settling chamber. The injected particles travelled from the beginning of the settling chamber and passed through the test section. Some of them could be caught in the filter at the end of the exhaust duct, while the others may deposit on the neighbourhood surfaces, e.g., foam block and test section/channel walls.

The most difficult task in conducting the fouling experiment is to repeat the same experiment multiple times due to massive time and cost consumptions. For this purpose, the settling chamber and the channel are purposely made of glass material. It is also designed to be easily dismantled, with an opening on the top wall of the test section. These designs allow us to clean all the particles in the settling chamber and the test section before conducting repetitive experiments. Three repetitive experiments were conducted for the highest and lowest blockages. A new foam sample was used in each experiment. However, it is important to note that it is impossible to have the first deposition on the same place within the porous structure. However, taking into account the whole deposition processes under the same operating conditions, the particle preferential deposition areas are still the same, regardless of the blockage ratios. Also, the statistical analysis to ensure the repeatability of the experiments was conducted in term of pressure drop comparison, with less than ± 6% deviation is found between those three repetitive experiments at the maximum injection period, t = 240 min.

A high-speed camera (Phantom v2011) was used to follow and study the particles movements when they were crossing the test section. Using the camera with Nikon mount lens (f = 50 mm, and maximum aperture, f/2.8), video recordings were acquired at 10,000 fps, with a resolution of 1024 × 768 pixels and exposure time of 30 μm. The recordings capture the particle movements over a two-dimensional plane of 0.195 m × 0.070 m field-of-view that is perpendicular to the camera position (located at one side of the test section). The camera was connected to a host computer, and Phantom Camera Control Software (PCC) was used to control the camera operation. Two multi-LED lights were mounted from both sides of the camera to obtain a clear view inside the test section. In this study, the particle movements are

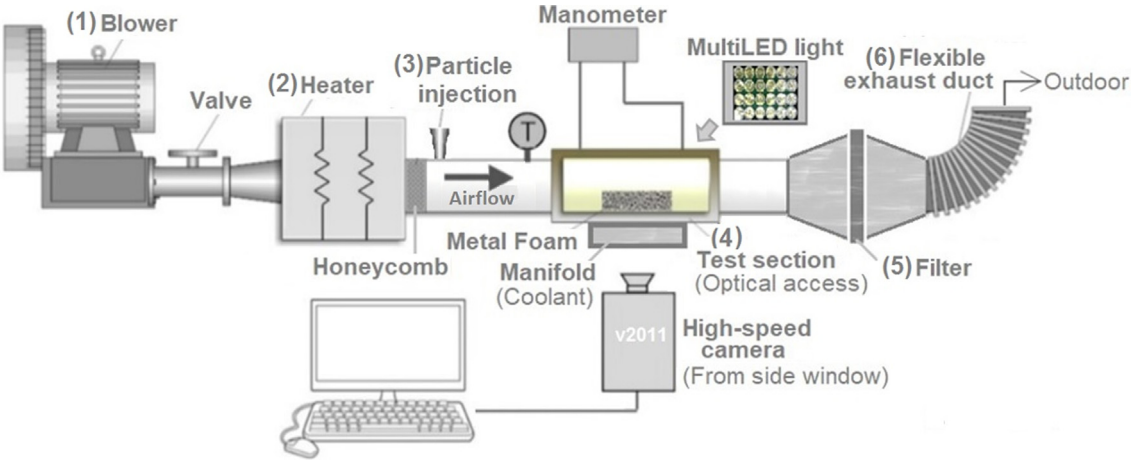

Fig. 1. Test rig with high-speed camera setup.

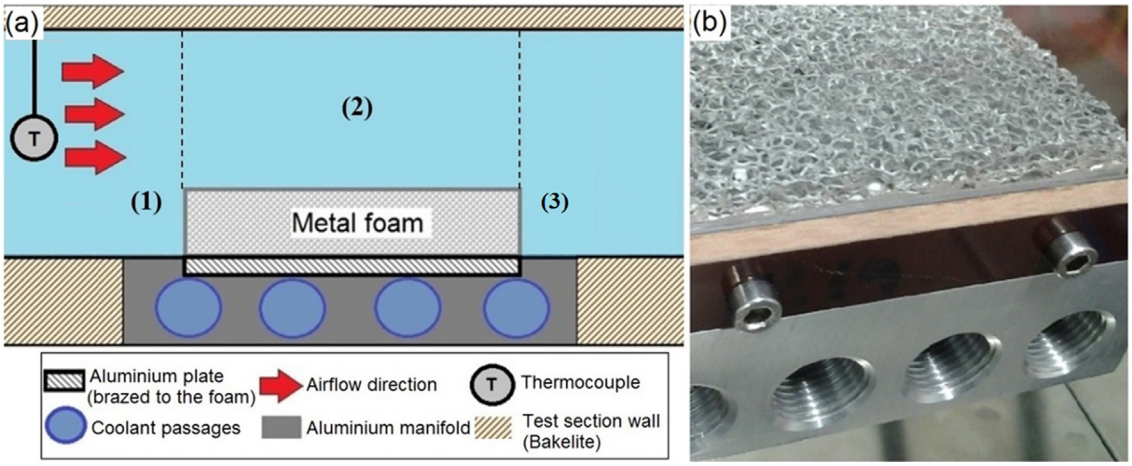

Fig. 2. (a) Cross-section of the test section with three ROIs (b) Partially filled section with a foam block - ROI 2.

expected to be primarily one-dimensional, following the main flow direction [25]. A short period of recordings (less than 30 min) was considered to avoid visual restrictions due to deposition of particles on the walls.

A refrigerated circulator (Julabo F25) was used to circulate coolant (50:50 water/ethylene glycol; 20 °C) in a closed loop at the bottom of the foam block to cause a thermophoretic deposition. The air gaps between the foam and aluminium manifold were eliminated by applying a thin layer of thermal conductive silicone paste (Omegatherm-201; k = 2.3 W/m K). The heater (3.0 kW) was also operated to increase the flow inlet temperature, $T_{air,in}$ from room temperature to 60 °C. All thermocouples (Type-K) were connected to a data logger (Omega RDXL8; accuracy: ± 0.5 °C). The particles were only injected after a steady state has been reached. It is when the temperature readings did not vary more than 0.5 °C during five-minute intervals. This took approximately 20–30 min depending on the flow velocity. Besides the in situ observation experiment, this study also conducted pressure drop measurements to understand the effects of fouling over time. Pressure taps (Sensirion, SDP-600 series; accuracy: ± 3%) were installed at the upstream and downstream of the foam block (L = 0.25 m). The measurements were taken at 30-minute intervals up to 240 min. The data are presented as a normalized pressure drop, $\Delta P_{fouled}/\Delta P_{\text{clean}}$, which is defined as pressure drop time-dependent values divided by the pressure drop under a clean condition. The pressure drop data under the clean condition is obtained from our previous study [22].

Ideally, a very long period experiment or an asymptotic fouling condition could not be used to distinguish the effects of a porous structure. Furthermore, the foam structures are expected to be completely covered with the particles, as found in [16]. In that case, understanding the morphology of the outer deposits layers is more important, instead of what buried inside for any possibility of mitigation and re-entrainment. Nevertheless, the present study was also conducted with the aims to determine the particle preferential deposition areas from the beginning of the fouling process and monitoring the process of particle removal, if there is any. The recorded videos are imported, and the particle size, trajectory, and velocity through those three regions; ROI 1, 2 and 3 (see Fig. 2(a)) are determined using Trackers software. This study considered the upstream (ROI 1) and downstream (ROI 3) regions are about 0.02 m and 0.07 m from the leading and rear edges of the foam block, respectively. These limited distances provided an acceptable resolution to obtain more accurate data, e.g., the particle size and particle travelled distance. The partially filled section (see Fig. 2(b)), where a foam block was positioned is called as ROI 2 in this study.

Note that, one of the main uncertainties in using the high speed camera is particle-position uncertainty [26], which would affect the results of particle trajectory and velocity. This study calibrated the video recordings/images using an image of a known object dimension [25]; a millimetre-ruler in this case. The image was used to determine the representative length of a pixel. The analyses were started with the adjustment of image sequences' brightness and sharpness to clearly identify individual particles. The two-dimensional velocity was also calculated based on the difference in a particle's position in two consecutive video frames, divided by the time interval between the frames. At least 100 particles were analysed for a statistical determination of the average particle velocity [26]. This study attempts to understand the effects of upward flow from the high blockage ratio and high PPI foam [24] on the particle velocity in the free stream region. In that case, Lf = 0.030 m is selected as a reference point. This study used an average sample size, N = 50 for every 0.010 m increments in the transverse direction. Also, the maximum uncertainty of the particle velocity is ± 1.2 m/s when using propagation of errors for those data

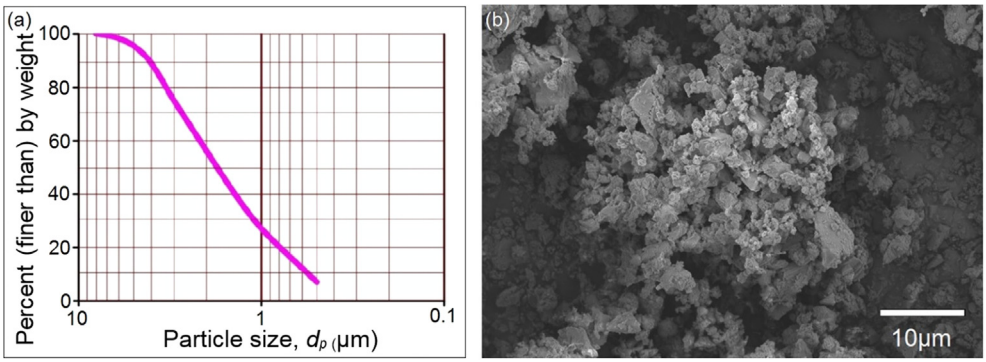

Fig. 3. (a) Particle size distribution in range of 0.5–8.0 μm [27] and (b) SEM image of $CaCO_3$.

obtained between two frame rates [26]. For a better understanding of the particle transport, some overlapping trajectories are purposely omitted, presenting only the average size particles of 300, 500 and 700 μm (± 100 μm), up to 20 min time frame.

2.2. Foulant and metal foam properties

This study used calcium carbonate ($CaCO_3$) to investigate the particulate fouling in the porous structure. These particles were chosen because of its ready availability and it poses neither health nor explosion hazards. Their speckling and brightness features also match the grayscale images of the high-speed camera. They were supplied by Omya Australia Pty. Limited [27] and their particle size distribution, and SEM image are shown in Fig. 3(a) and (b), respectively. Based on a cumulative percentage, the particle size is ranging from 0.5 to 8 μm with the mean diameter, $\overline{d_p}$ is 1.8 μm (D50) [27]. However, it was noted during experiments the particles can easily agglomerate as moving through the particle feeder and the settling chamber. Our online data (video recordings) shows a larger particle size distribution in the air motion, up to 700 ± 100 μm. These equivalent particle sizes were determined from their projected area diameter [28] in the two-dimensional plane. For the sake of simplicity, the particle shape was assumed spherical, where the effects of particle polydispersity and irregularities (Fig. 3(b)) are neglected in this study.

Note that there are also fine particles in the test section. However, quantitative analyses are difficult because of their low intensity and brightness in the video recordings. The fine particles were assumed to accurately follow the fluid streamlines while the other particles with their sizes in between 100 and 800 μm were characterized to determine their trajectories and velocities. The widely dispersed particle size is required in this study to suit the randomly distributed pores, different pore diameters up to 2.5 mm and very small ligament diameters (up to 6 times smaller than the pore diameter). In addition, our in-situ observations were conducted to investigate the deposition processes in the porous structure of the metal foam block and its outer region. The metal foams were purchased from China Beihai Building Material Co., Ltd. [22], with the details in listed in Table 1. In this study, different pore densities (10 and 30 PPI) were used to investigate the influence of porous structure on the propensity of fouling.

3. Results and discussion

The particle trajectories would be helpful in identifying the particle preferential deposition area in the partially filled section. The results show popular pathways for different size particles, which are more likely to deposit once come into collision with the foam block. The dominant deposition mechanisms can be also determined based on the particle trajectories. The high inertia particles are expected to stay on their original direction. While the particles that move toward the channel floor may experience significant gravitational influences. As the deposition layer is increasing with the particle injection, the pressure drop performances will be affected. Thus, the pressure drops of the partially filled channel are also presented in this study.

3.1. Particle trajectories and velocities

As expected, there are fewer particles found in the regions close to the top wall. Thus, this study combined at least 50 particles (of the same size) from adjacent transverse positions to have a statistically sufficient database [29]. The particle trajectories over the two-dimensional planes along the partially filled channel with different PPIs are obtained from the particle tracking analyses. In general, the particle trajectories are influenced by their densities (variety in sizes) and the results could be also different from the fluid (air) streamlines [22] and velocity fields [24], which had been measured using a particle image velocimetry with 3 μm seeding particles. Fig. 4 shows some of the particle trajectories are consistent with the flow motion [24], while the others would deviate from the mean streamlines, revealing their complex motion. Regardless of pore density, four main situations occur in the partially filled channel; (1) particle collision and deposition on/within the foam block, (2) particles breakage, (3) particles exit through the fluid/foam interface, and (4) particles transport through the ROIs without any deposition. For the experiments with a low blockage ratio, h/H ≤ 0.13, most of the particles would move towards the end of the test section, supporting our findings on the insignificant effects of low blockage ratio [24]. However, the partially filled channel with a significant blockage ratio, h/H = 0.39, would restrict the particle movements in the lower region, as expected (see Fig. 4(a) and (b)). As the particle-laden flow passes through ROI 1, direct particle impaction with the frontal area (ligament surfaces) of the foam block is possible. Consequently, some of them deposit on the bottom surface of ROI 1, while the others could successfully enter the porous region, depending on the particle and the subjected pore sizes.

Some particles also tend to avoid the foam block, following the fluid streamlines into the non-porous region, particularly for the smaller particles, $\overline{d}_p \leq$ 500 μm. Interestingly, Fig. 4(a) shows the bend degree (curvilinear motion) of the particle trajectories with 10 PPI foam are stronger than 30 PPI foam as the particle is moving away from the fluid-foam interface. This suggests the horizontal flow in the free stream region of 10 PPI is significant. Meanwhile, Fig. 4(b) shows some trajectories ($\overline{d}_p < \overline{d}_{\text{pore}}$)with 30 PPI foam have upward deviations from the fluid streamlines in a region near to the leading edge. Unlike the 10 PPI foam that allows more particles to come out along the interface, the particle trajectories with 30 PPI foam only appear in the regions near to the leading and rear edges. This phenomenon could be influenced by the flow behaviours in the partially filled channel. For the 30 PPI foam with higher restrictions, it is known that the flow inside its porous structure could lose its momentum and exit through the interface, specifically a region about one-third from the leading edge [24]. Our previous study [24] also found a large recirculation zone behind the foam block, originating from the foam itself. Thus, the present particle laden flow shows the similar flow behaviours, forcing the particles to transport in the same manner. Regardless of the foam pore density, it is also important to note that many particles trajectories show direct impact on the roof of the test section. Those particles deposit and accumulate on that surface instead of moving toward the exhaust duct.

In another opinion, the particles trajectories on the interface may also represent the detachment of the deposited particles as the flow is passing through. Because of its larger pores, 10 PPI shows different size particles up to 700 μm are exiting through the interface. While, most of the smaller size particles (less than 500 μm) are found with the 30 PPI foam. Most likely, this phenomenon is experienced by the naturally small particles ($\overline{d}_p < \overline{d}_{\text{pore}}$), or a result of particle breakage episode in the porous structure. Note that it is impossible for those particles with a larger size than the pore diameter ($\overline{d}_p > \overline{d}_{\text{pore}}$) to penetrate into the porous region. Unless the particle breakage incident is happening, as they hit the foam-ligament surfaces. Interestingly, this study noticed that the particle breakage could be a natural event in this case,

Table 1
Metal foam microstructural and geometrical properties.

Parameter	Sample 1	Sample 2
Pore density (PPI)	10	30
Ligament diameter, d_l (m)	0.00044	0.00027
Pore diameter, d_{pore} (m)	0.00256	0.00087
Porosity, ε (–)	0.82 – 0.91	0.88–0.94
Permeability, $K \times 10^{-7}$ (m^2)	1.54–1.65	0.35–0.37
Foam height, h (m)	0.004, 0.01, 0.03	
Blockage ratio, h/H	0.05, 0.13, 0.39	
Foam length, Lf (m)	0.09	
Foam width, wf (m)	0.10	

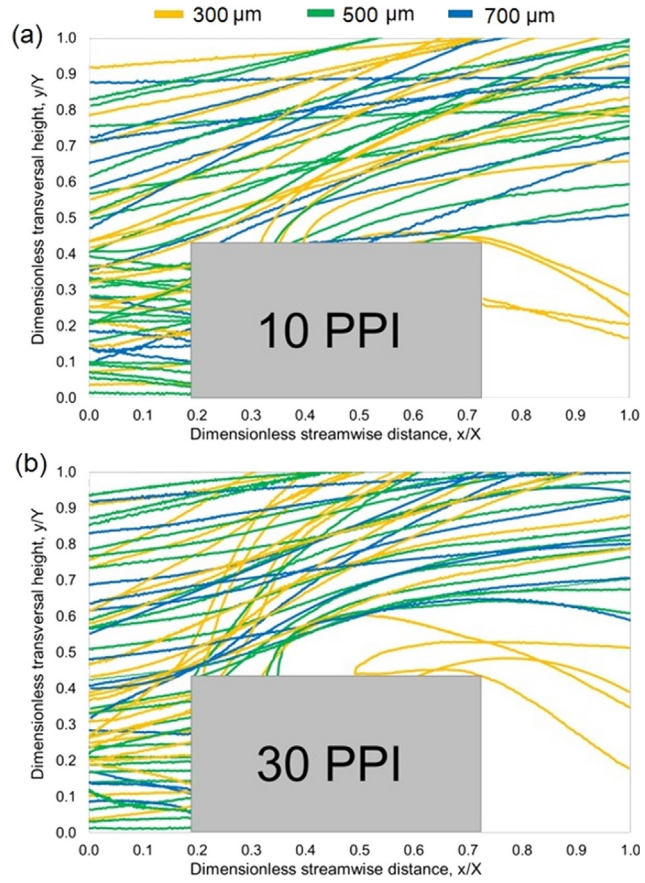

Fig. 4. Particle motion trajectories in the partially filled channel (flow direction from left to right).

considering the nature of our particle characteristics and the interconnected pore-ligament networks. This topic will be discussed further in the following section.

It is also noticeable in Fig. 4(a) on how the particle keeps its inertia and passing linearly through both porous and non-porous (free stream) regions. This, probably due to a small disturbance in the free stream region as more flow prefers to enter the porous structure of 10 PPI. If considering the flow behaviors inside the porous structures [24], the 10 PPI foam seems to have a higher capability to accommodate more particles. These higher amounts of incoming flows into the porous region is also a good indicator that the deposited particles could be carried away out of the porous region. However, very few particles exit the rear ends of the 10 PPI foam, and there is no particle (visible size from the on-line data) is coming out from the 30 PPI foam. In that case, the 30 PPI foam with smaller pores could have blocked or trapped the particles, and the very low velocity at the downstream region (due to the existence of a recirculation zone) could not bring back the particles towards the foam, as shown in ROI 3, Fig. 4(b). It is also possible because of a stagnant region in the high PPI foam [24]. However, the 10 PPI foam with larger pores may only allow the particle to pass through its porous structure up to a certain period. In summary, those two PPIs show different particle movements in ROI 2 (the non-porous region) and ROI 3.

Fig. 5 depicts normalized particle velocity with different PPIs, measured on the top of the foam block at Lf = 0.030 m. The average particle velocity is normalized by the mean inlet velocity, u_o. Because of the limited visual inside the porous region, the foam interface is considered as the starting point for the particles. Also, note that Fig. 5 is based on the field-of-view of the camera. Based on the decreasing profiles in adjacent regions near to the top wall (Fig. 5(a)), we could assume a no-slip condition for the particle velocity on that surface. Only small friction effects are expected because of the smooth material (quartz) of the top wall.

In general, we can observe the particles accumulate in the low-speed streaks that near to the foam interface. The lower velocity is possibly due to different flow regime [24], where a boundary layer appears on the foam interface, regardless of pore density. As expected, the smallest particle, $\overline{d}_p$ = 300 µm shows a lower velocity as compared to those two larger particles, especially in the adjacent region to the interface. The rests in Fig. 5(a) show similar profiles with only a small difference in value. The largest particle, $\overline{d}_p$ = 700 µm, which is supposed to have the highest density is moving a little bit faster as compared to the others.

Meanwhile, Fig. 5(b) with the 30 PPI foam shows virtually a linear velocity increment, starting from y/Y = 0.6 for those two larger size particles. Interestingly, their velocity is slightly lower as compared to those particles with 10 PPI foam. Those large particles are probably trying to keep their inertia towards the top wall, but declining in speed due to the effect of secondary flow that only appear in the free stream region of 30 PPI foam [24]. Even though the large particles might keep their directions, the upwards flow motion may have some influences on their velocity and momentum. In a case with the smallest particle, $\overline{d}_p$ = 300 µm, the upwards flow motion influences both the trajectories (see Fig. 4(b)) and velocity. Most of the smallest particles at the point of interest, (Lf ~ 0.030 m) show a tendency to move upwards and to verge slowly in the streamwise direction. This, however, contributes to a lower velocity (based on the particle distance between two frames). Their upward motions also suggest insignificant drag effects and the existence of slip velocity around these small size particles. The variations in the trajectories and velocity are expected to cause a

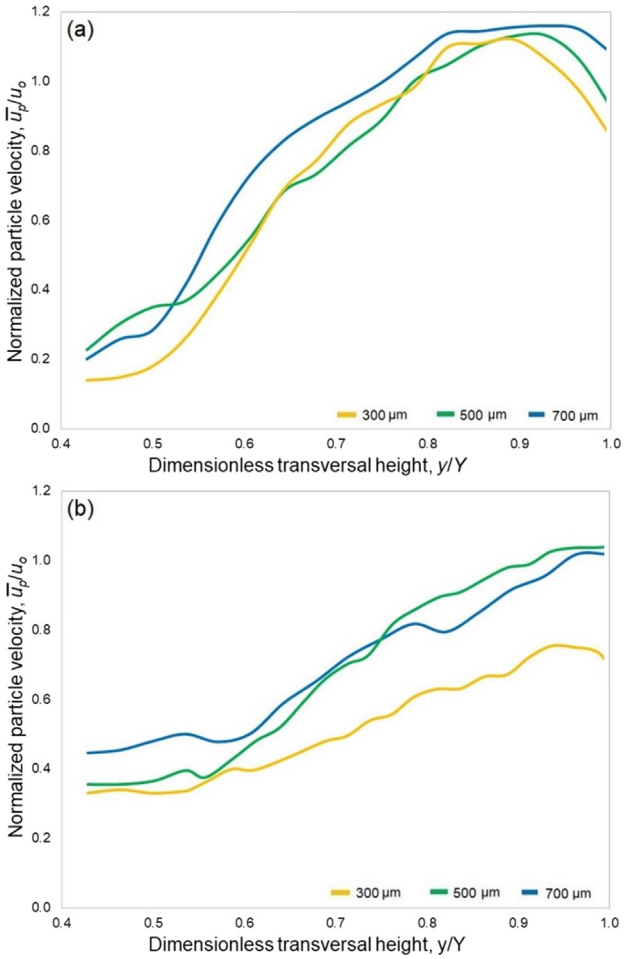

Fig. 5. Normalized particle velocity in ROI 2 with h/H = 0.39 (a) 10 PPI (b) 30 PPI.

complicated deposition process within the porous structure of the metal foam.

The partially filled channel with porous structure caused high turbulence intensities, especially from x/X = 0.25–0.72 as shown in Fig. 6. The turbulence intensities increase significantly regardless of the pore density, with the 30 PPI foam shows higher values up to 30%, most probably because of additional upward flow motions from the interface. In addition to the secondary flows, the presence of both particle-turbulence and particle-wall interactions (at the foam-fluid interface) also affect the particle motions through additional lift forces, for example Magnus force [30] and Saffman force [31]. It is important to note that the pressure differences around the particle and shear fluid at the interface may cause particle rotations and induced lift force that move the particles away into the free stream region. However, our experiment setup could not directly capture the rotation of the particle and angular velocity, thus a high-speed stereoscopic imaging [32] will be a better approach to study the Magnus effects.

3.2. Particle preferential deposition areas, transport and deposition mechanisms

Our findings support the ideas by Hooman et al. [7] that small particles could pass through the pore network with some of them may deposit on the ligaments and partially block the pathways, while large particles tend to sit and clog the pores. However, our results also show those phenomena are subjected to the type of particles or foulant, besides the interconnected pores. To have a clear view on the relationship between the particle and the porous structure, a series of raw images (Fig. 7) that describes the process of particle transport from the upstream region towards the foam block is also included. Note that the time, (t) in Fig. 7 is the travelling period from one point to another point in 30 fps video recordings, which is not the real-time of particle motion during the experiment.

Fig. 7(a)–(c) shows how the particle is approaching the foam block. The particle enters the porous structure of the foam and disappears for a while before coming out from the top surface (Fig. 7(d)). Even though the carrier (particle laden flow) is passing through the porous structure, the particle collides with the ligaments and breaking into several pieces. A part of those pieces is being carried away by the incoming flow and dispersed into the free stream region. While some of them may deposit on the foam surface. Also note, the detachment of the deposits by the impact of the incoming flow is also possible, suggesting this as one of the important transport mechanism in the partially filled channel. This phenomenon offers a high possibility to make use of the porous structure to remove the unwanted particles. The particle/agglomerate rigidity and flow impact must be taken into account when considering the metal foam application under a fouled condition. Most prominently, due to randomness and interconnected pores, the penetrated particles could be caught inside the porous region. Without proper design, the foam itself could act as a trap or filter to the particles.

As one would expect, the preferential deposition areas are significantly depending on the foam arrangement and its geometrical design. The effects of our arrangement on the deposition process are schematically described in Fig. 8. For the low blockage ratio case (Fig. 8(a)), for example, h/H = 0.13, it is found that the preferential deposition area is located at the top surface of foam block, as most of the particle-laden flow could successfully pass through the partially filled section (ROI 2). The horizontal flow encourages the shear effect on the foam interface. Even though this shear may also contribute to the detachment of particles, the deposition rate is undisputable higher in this case. The deposition could further be increased because of the gravitational forces. While, the preferential deposition area for the high blockage ratio (Fig. 8(b)) is right in front of the foam block, within ROI 1. Note that the specific size particles ($\overline{d}_p < \overline{d}_{\text{pore}}$) may either penetrate into the porous region, or colliding with the ligament restrictions, get deposited on the foam surfaces or the bottom of RO1 region. Due to the prolonged injection time, the deposited particles started to accumulate in ROI 1, resulting in completely blocked passages (frontal area of the foam block) into the porous region.

These accumulated particles form a slope or triangular-shaped deposits right in front of the foam block, which could be obviously seen with the high blockage ratio. From that point, the flow tends to choose the free stream region. Note that the deposits in ROI 1 could either, (1) stick there for a very long time or (2) detaching from that slope due to lifting or rolling effects because of the impact of the incoming flow. Within this injection period, we could conclude that the upstream region (ROI 1) and the leading edge are the preferential deposition areas for the high blockage ratio, regardless of pore density (PPI). In this study, most of the large particles do not follow the fluid streamlines [22,24]. Thus, the inertial impaction is the dominant mechanism for the high blockage ratio. However, the thermophoresis is unlikely important for the high blockage ratio, due to the presence of a local thermal equilibrium between the upper region of the foam block and fluid phase [24].

At the microscopic level (Fig. 9), we could see that those particles either get deposited on the bottom surface of the aluminum plate or stick on the ligaments. Different size particles ($d_p < d_{pore}$) found on the bare plate (see Fig. 9(a)) and with a close observation on Fig. 9(b), one can realise that the depositions on the ligament surfaces are non-uniform and they are subjected to the orientations of the ligament surface. Those exposed areas to the flow (circled in red colour) could have a thicker deposition as compared to the hidden areas at the beginning of the fouling process. This proved that the assumption of uniform deposition layers in the porous structure [7,9] is not always true in a real practice.

Even though the deposition layer is building up and filling up the pores, the structure of the deposition layers itself are non-uniform, at least in this case. It is worthy to note that these initial depositions are important, as they are more likely to influence the subsequent deposition processes, by providing a higher adhesion force and more restrictions to the other particle motions. This, however, is better observed after more particles are injected into the system, as shown in Fig. 10.

In term of PPIs, the 30 PPI foam is blocked faster due to its more restrictions and smaller pores than 10 PPI foam. Fig. 10(a) shows that the high PPI foam is easily filled with the particles, but more unclogged areas with 10 PPI foam, as shown in Fig. 10(b). It also clearly seen with the 10 PPI foam that there exists strong adhesion between particles, as the particles tend to deposit on the same spot. Another possibility is the effects of internal or tortuous flows, where the 10 PPI foam allows more flow to pass through its pores, avoiding or detaching the deposits. This study agreed with the findings from another literature [16], that more deposition of the fine particles, e.g., soot particles on the upper ligament surface (on the interface) as compared to the lower ligaments of a more porous foam. With the low blockage ratio, h/H = 0.13, there is a

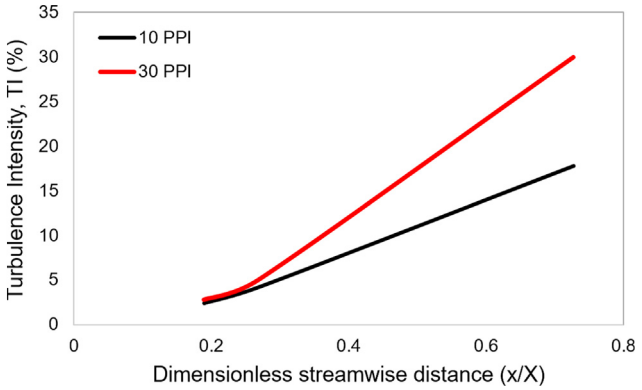

Fig. 6. Turbulence intensity in the partially filled section with 10 PPI and 30 PPI (Re_{Dh} = 36,000).

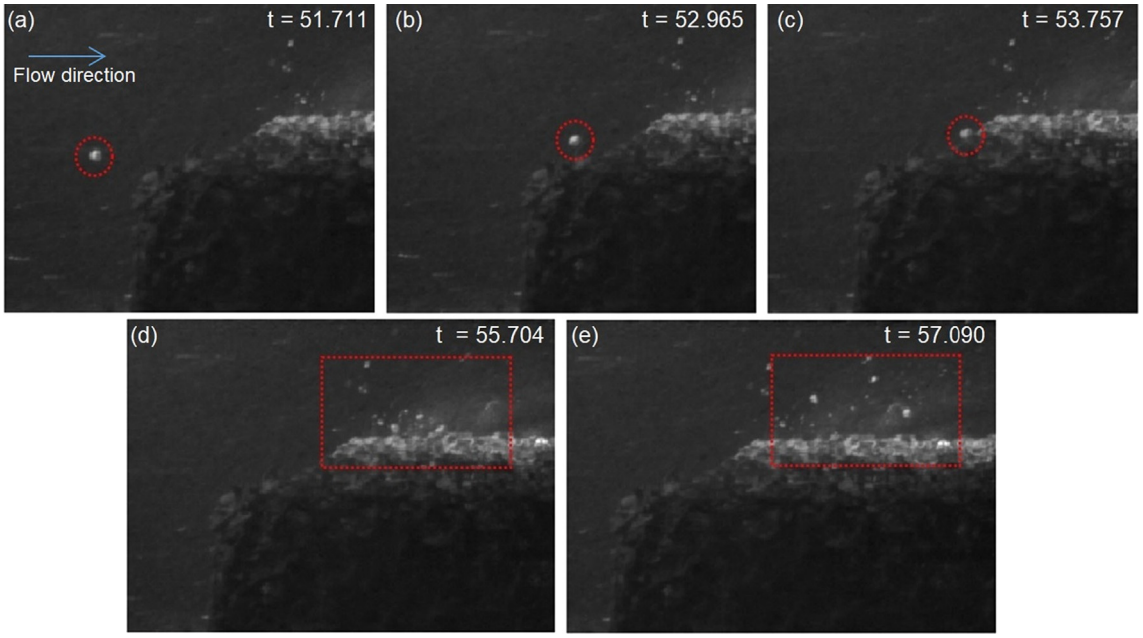

Fig. 7. Particle transport, breakage and dispersion.

high possibility that the dominant deposition mechanism is thermophoresis at the beginning of the fouling process (t = 30 min). Those fine particles were attracted to the heated aluminium ligament and plate surface as shown in Fig. 9. Once it started to accumulate more deposits, the thermophoresis is no longer becomes the dominant mechanism. This transport mechanism is possible as our particles could be as small as 0.5 μm (see Fig. 3 (a)). The particles tend to deposit on the ligament surfaces, obviously seen with the 10 PPI foam. Our previous study [24] found that the coolant at the bottom of foam block (h/H = 0.13) caused a low temperature region in the entire foam block. In that case, the fluid molecules from the hot sides (upstream and free stream regions) have a higher velocity than fluid molecules near or inside the foam block. Consequently, the fine particles may experience a thermophoretic force, while the large particles would keep their inertia and move towards the downstream region of this setup.

3.3. Pressure drop performances

Fig. 11 depicts normalized pressure drops for different PPIs and blockage ratio, h/H = 0.05–0.39 in the test section at inlet velocity, u_o = 6.2 m/s. Our result with h/H = 0.39 is also compared with another literature [8] that considered 20 and 40 PPI metal foams as a potential EGR cooler. Regardless of the PPIs and blockage ratio, the normalized pressure drops are only increasing towards the end of injection time of 240 min. It is noticeable that the pressure drop values are fluctuated before subsequently reaching a similar value, regardless of PPI and blockage ratio. It was expected as the experiment deals with unpredicted deposition process over the complicated structure of the metal foam. Later, the 10 and 30 PPI foams show similar pressure drops beyond 200 min of particle injection, suggesting significant depositions in the porous structure at that time. Interestingly, at the beginning of the fouling process, the pressure drops of 10 PPI foam is mostly higher than 30 PPI foams, except for h/H = 0.05 (Fig. 11(a)).

One would expect to see the pressure drop of 30 PPI is higher than 10 PPI foam, as a result of its more substantial pore-ligaments restrictions with a higher tendency to trap more particles. However, due to the more porous structure of the 10 PPI foam, it could accommodate more particles further inside (streamwise direction). Meanwhile, the 30 PPI foam could have more depositions over its frontal area. This effect may cause fluctuated, and disturbance flows in the 10 PPI foam, producing a higher pressure drops at the beginning of the fouling process as compared to 30 PPI foam. Also, the 10 PPI foam with larger pores causes more particles (various sizes) to enter and escape its porous structure (Fig. 4(b)). Those trapped particles inside the porous structure, however, may influence the internal surface roughness and frictional effects on the pressure drops. Interesting, the pressure drops also decrease for a

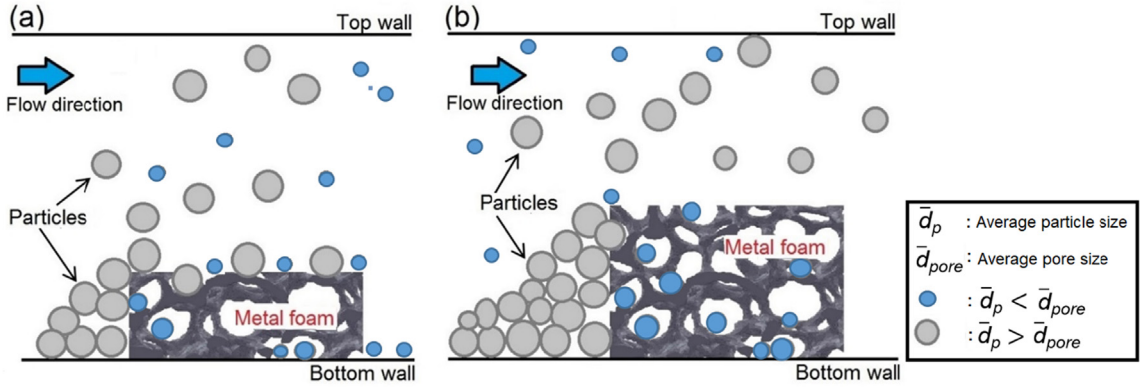

Fig. 8. Illustration of particle deposition across the partially filled section (a) low blockage ratio and (b) high blockage ratio.

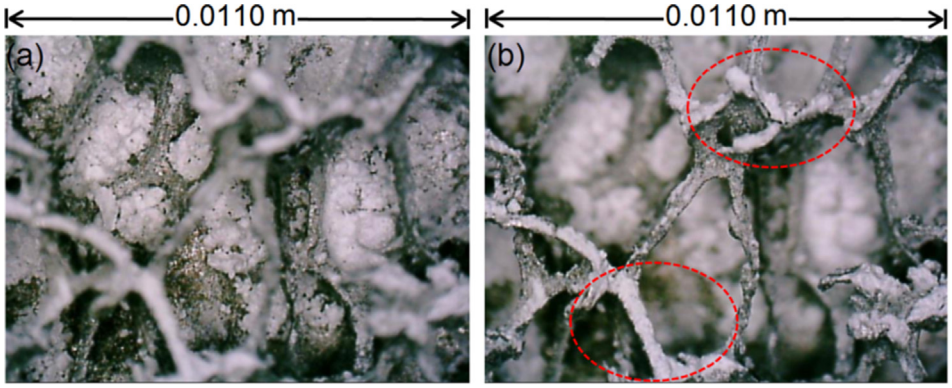

Fig. 9. Microscope images of 10 PPI foam at the same location (a) Deposition on the bare plate (b) Deposition on the ligaments (Flow from the right to left direction).

while, around 80–120 min before increasing again. Probably, as the frontal area of the foam blocks is blocked, the foams mimic a solid block behaviour with no internal friction effects. As the injection continued, more particles could be pushed further into the foam block that increase the pressure drops again. The deposition within the porous region may reduce the permeability of the porous structure and affect the internal flow behaviours. However, this probably more dominant with the 10 PPI foam. Also noted, both PPIs are subjected to a non-uniform distribution of the particles within their porous structure as a result of their internal flow behaviours [24]. These could be the reasons for these fluctuation values of the pressure drops, among the other factors which are not yet discovered at this point of research.

Interestingly, the normalized pressure drops with h/H = 0.13 show the highest values as compared to the other blockage ratio, h/H = 0.05 and 0.39. The high blockage ratio setup has more deposition in the upstream region and the adjacent regions to the leading edge, but lesser particles in the rear region (according to the trajectories in Fig. 4). Meanwhile, the low blockage ratio is subjected to more deposition on the top surface and inside the pores. Hence, the significant fouled structure tends to cause a substantial increase in the pressure drop. However, as the fouling layers intensify over time, the microstructural effects become insignificant, resulting in a similar pressure drop value. By comparing our results, h/H = 0.39 with [8], the normalized pressure drops are quite similar, except the significant drops in the pressure drop at a specified period. Most probably, since our total pressure drop are affected by the minor losses at the upstream and downstream, the pressure drops could be easily affected by the presence of the deposits at the upstream region. Thus, mimicking the lower pressure drop value of a solid block [22], at one time before experiencing an increase of pressure drop due to the deposition.

4. Conclusion

In this study, particle transport and deposition processes were studied in a partial filled channel by means of direct observation using video recordings. The remarkable findings from this study are summarized as follows:

(a) The particle size is one of the important parameters in characterizing the particle trajectories in the partially filled channel. The large particles keep their inertia, and tend to hit the obstacle in the pathways, if there is any. While the fine particles follow the fluid streamlines.
(b) The particle deposition on/within the porous structure are also highly dependent on the particle size or in the opposite view, subjected to the pore and ligament sizes. The high blockage ratio causes more depositions in the upstream region, regardless of PPIs. However, there almost no deposition behind the block, probably due to very low velocity in that region.
(c) Inertial impaction is the dominant mechanism for the high blockage ratio. The preferential deposition area for the low blockage ratio is the top surface of the foam block, attributed to the effects of thermophoresis and drag forces.
(d) Some particles detach or exiting into the free stream region through the fluid-foam interface. The particles tend to follow the fluid behaviours, with some of them could break into smaller pieces as colliding with the pore-ligament networks. The existence of Magnus forces and Saffman forces should not be ruled out, as some of the trajectories also show upward particle motions at the interface region.
(e) Deposition causes a fluctuated pressure drop at the initial stage before reaching a similar value, regardless of PPIs. The deposition within the porous structure and over the frontal area of the foam block could be the main reasons for these fluctuating values.

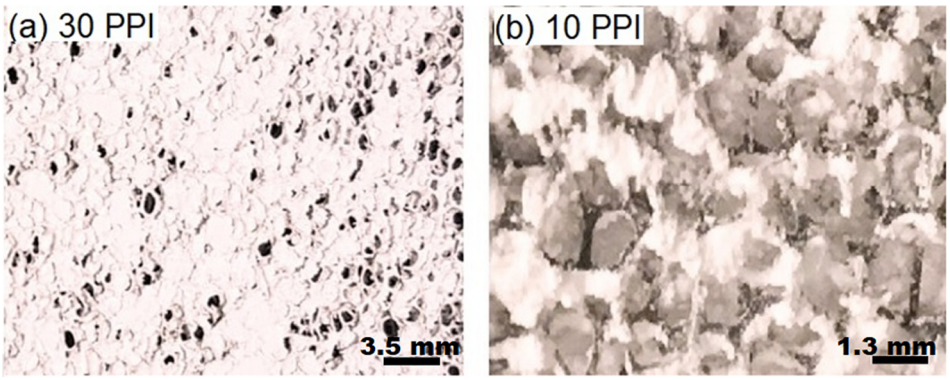

Fig. 10. Particle deposition on the top surface of the foam block (h/H = 0.13) with different pore densities.

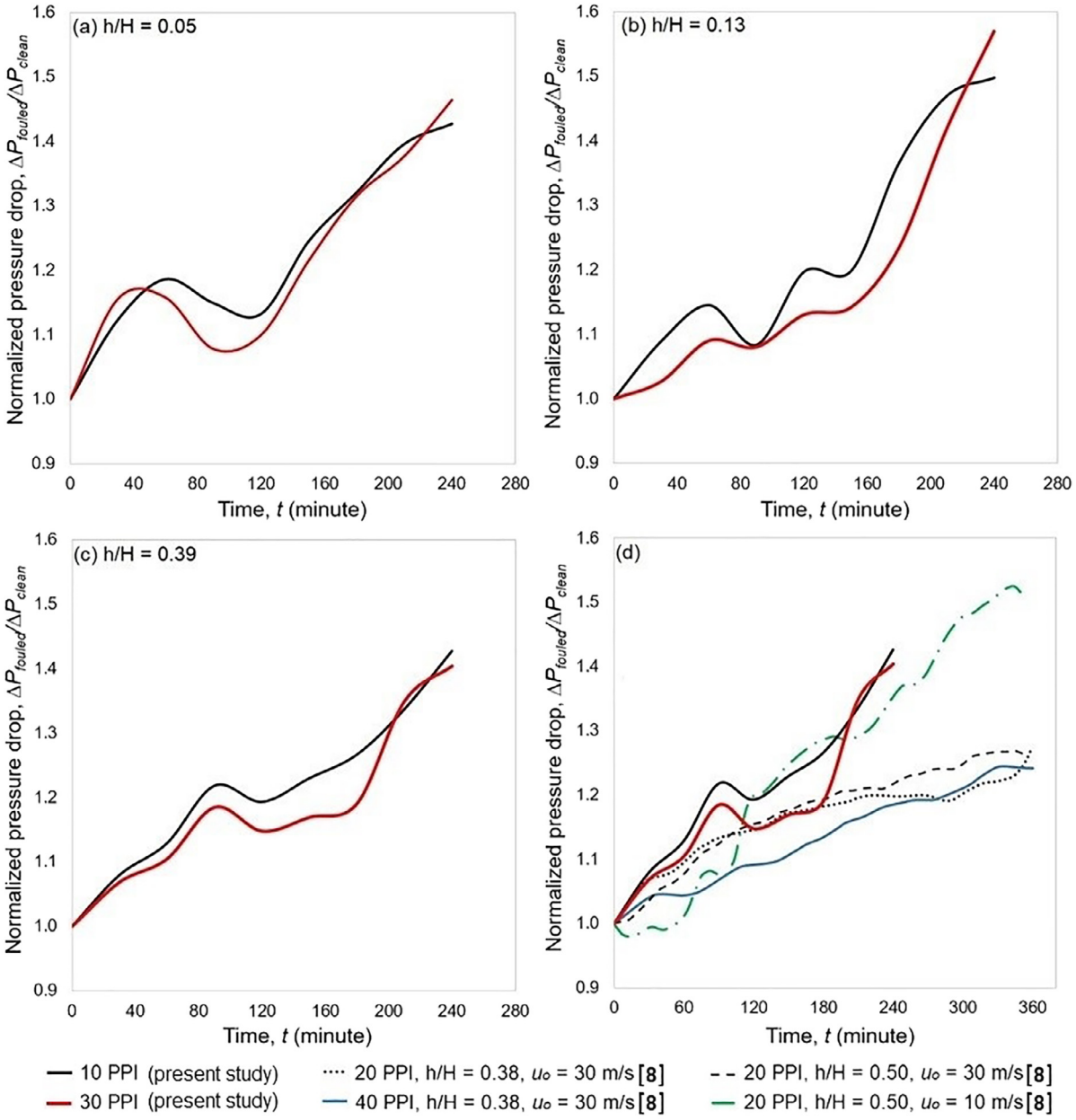

Fig. 11. Normalized pressure drop of partially filled channel with different PPIs and blockage ratio (a) h/H = 0.05, (b) h/H = 0.13, (c) h/H = 0.39 and (d) Comparison of present data with existing literature.

5. Suggestion for future work

The present work is two-dimensional imaging studies, with the results are limited in the range of condition examined. Therefore, three-dimensional measurements that could provide a full understanding of particle transport, including the span-wise effects is called for. It is also important to perform further mathematical analysis to understand the combination forces acting on the particles in lateral and streamwise directions. As the high PPI foam seems to act as a filter, a highly compact metal foam heat exchanger could be inappropriate for a dusty environment, expecting severe fouling and difficulty in the cleaning processes. However, a proper foam arrangement with a suitable pore diameter and flow velocity could be a promising design to enhance the particle removal process. This, however, also depend on the particle characteristics such as particle size and density. The weighted on how good the interconnected pore-ligament network to mitigate fouling should be explored, e.g. the relationship of particle laden flows with different particle Reynolds numbers and a ratio of particle size and pore diameters. A depth knowledge of the particle-detachment process is fundamental to the development of fouling-metal foam models and their predictive capabilities.

Declaration of Competing Interest

The authors declared that there is no conflict of interest.

Acknowledgement

Authors acknowledge Omya Australia Pty. Limited as a supplier for the $CaCO_3$ particles. The content of this paper is the sole responsibility of its authors, and it does not represent the views of the supplier.

The contribution of Dr. Mingyuan Lu (Associate Lecturer, School of Mechanical and Mining Engineering, UQ) in producing the SEM image is gratefully acknowledged.

References

[1] A. Muley, C. Kiser, B. Sundén, R.K. Shah, Foam heat exchangers: a technology assessment, Heat Transf. Eng. 33 (1) (2012) 42–51.

[2] Z.-B. Liu, Y.-L. He, Y.-F. Yang, J.-Y. Fei, Experimental study on heat transfer and pressure drop of supercritical CO2 cooled in a large tube, Int. J. Heat Mass Transf. 85 (2015) 679–693.

[3] Y. Li, S. Wang, Y. Zhao, Experimental study on heat transfer enhancement of gas tube partially filled with metal foam, Exp. Therm. Fluid Sci. 97 (April) (2018) 408–416.

[4] M.P. Orihuela, F. Shikh Anuar, I.A. Abdi, M. Odabaee, K. Hooman, Thermohydraulics of a metal foam-filled annulus, Int. J. Heat Mass Transf. 117 (2018) 95–106.

[5] F. Shikh Anuar, M.R. Malayeri, K. Hooman, Particulate fouling and challenges of metal foam heat exchangers, Heat Transf. Eng. 38 (7–8) (2017) 730–742.

[6] X.-H. Han, Q. Wang, Y.-G. Park, C. T'Joen, A. Sommers, A. Jacobi, A review of metal foam and metal matrix composites for heat exchangers and heat sinks, Heat Transf. Eng. 33 (12) (2012) 991–1009.

[7] K. Hooman, A. Tamayol, M.R. Malayeri, Impact of particulate deposition on the thermohydraulic performance of metal foam heat exchangers: A simplified theoretical model, J. Heat Transfer 134 (9) (2012) 092601.

[8] K. Hooman, M.R. Malayeri, Metal foams as gas coolers for exhaust gas recirculation systems subjected to particulate fouling, Energy Convers. Manage. 117 (2016) 475–481.

[9] M. Odabaee, M. De Paepe, P. De Jaeger, C. T'Joen, K. Hooman, Particle deposition effects on heat transfer from a metal foam-wrapped tube bundle, Int. J. Numer. Methods Heat Fluid Flow 23 (1) (2013) 74–87.

[10] E. Sauret, S.C. Saha, Y. Gu, Numerical simulations of particle deposition in metal foam heat exchangers, Int. J. Comput. Mater. Sci. Eng. 2 (3&4) (2013) 1350016.

[11] S.T.W. Kuruneru, E. Sauret, S.C. Saha, Y.T. Gu, Numerical investigation of the temporal evolution of particulate fouling in metal foams for air-cooled heat exchangers, Appl. Energy 184 (2016) 531–547.

[12] S.T.W. Kuruneru, E. Sauret, K. Vafai, S.C. Saha, Y.T. Gu, Analysis of particle-laden fluid flows, tortuosity and particle-fluid behaviour in metal foam heat exchangers, Chem. Eng. Sci. 172 (2017) 677–687.

[13] E. Sauret, K. Hooman, Particle size distribution effects on preferential deposition areas in metal foam wrapped tube bundle, Int. J. Heat Mass Transf. 79 (2014) 905–915.

[14] P. Clark, K.A. Koehler, J. Volckens, An improved model for particle deposition in porous foams, J. Aerosol Sci. 40 (7) (2009) 563–572.

[15] H.D. Ackermann, Experimental Investigation of Fouling in various Exhaust Gas Recirculation Coolers, ITW-Thesis, University of Stuttgart, Germany, 2012.

[16] J. Kahle, Experimental investigation of deposit formation in foam structured EGR coolers, ITW-Thesis, University of Stuttgart, Germany, 2012.

[17] S.T. Wickramasooriya Kuruneru, E. Sauret, S.C. Saha, Y.T. Gu, A novel experimental method to assess particle deposition in idealized porous channels, Heat Transf. Eng. 38 (11–12) (2017) 1008–1017.

[18] C. T'Joen, P. De Jaeger, H. Huisseune, S. Van Herzeele, N. Vorst, M. De Paepe, Thermo-hydraulic study of a single row heat exchanger consisting of metal foam covered round tubes, Int. J. Heat Mass Transf. 53 (15–16) (2010) 3262–3274.

[19] S.T.W. Kuruneru, E. Sauret, C.S. Suvash, Y.T. Gu, K. Hooman, A novel experiment method to asses industrial aerosol deposition in idealised porous channels, in: 17th IAHR Int. Conf. Cool. Tower Heat Exch., no. September, p. September, 2015.

[20] S.T.W. Kuruneru, E. Sauret, C. Saha, Y. Gu, Poly-disperse particle transport and deposition in idealized porous channels, in: 2nd Australasian Conference on Computational Mechanics, 2015, no. December.

[21] S.T. Wickramasooriya Kuruneru, E. Sauret, C.S. Suvash, Y.T. Gu, An FVM-DEM assessment of particle deposition in low-porosity foams with circular strut cross sections for electronics cooling applications, in: R. Aust. Chem. Institute, Chemeca Conf. 2017, no. July, pp. 23–26, 2017.

[22] F. Shikh Anuar, I. Ashtiani Abdi, M. Odabaee, K. Hooman, Experimental study of fluid flow behaviour and pressure drop in channels partially filled with metal foams, Exp. Therm. Fluid Sci. 99 (2018) 117–128.

[23] M. Odabaee, S. Mancin, K. Hooman, Metal foam heat exchangers for thermal management of fuel cell systems – An experimental study, Exp. Therm. Fluid Sci. 51 (Nov. 2013) 214–219.

[24] F. Shikh Anuar, I. Ashtiani Abdi, K. Hooman, Flow visualization study of partially filled channel with aluminium foam block, Int. J. Heat Mass Transf. 127 (2018) 1197–1211.

[25] R. Lindeboom, G. Smith, D. Jeison, H. Temmink, J.B. van Lier, Application of high speed imaging as a novel tool to study particle dynamics in tubular membrane systems, J. Memb. Sci. 368 (1–2) (2011) 95–99.

[26] Y. Feng, J. Goree, B. Liu, Errors in particle tracking velocimetry with high-speed cameras, Rev. Sci. Instrum. 82 (5) (2011).

[27] Omya Australia Pty. Limited, "Cement Based Products." [Online]. Available: https://www.omya.com/Pages/au/en/cement_based_products.aspx (Accessed: 26-Feb-2018).

[28] W. Pabst, E. Gregorova, Characterization of particles and particle systems, ICT Prague (2007) 1–122.

[29] D. Kaftori, G. Hetsroni, S. Banerjee, Particle behavior in the turbulent boundary layer. II. Velocity and distribution profiles, Phys. Fluids 7 (5) (1995) 1107–1121.

[30] M.D. Manshadi, The importance of turbulence in assessment of wind tunnel flow quality, in: Wind Tunnels and Experimental Fluid Dynamics Research, 2011, pp. 261–278.

[31] P.G. Saffman, The lift on a small sphere in a slow shear flow, J. Fluid Mech. 22 (2) (1965) 385–400.

[32] Y.H. Tee, D. Barros, E.K. Longmire, Translation and rotation of a spherical particle in a turbulent boundary layer, in: 19th International Symposium on the Application of Laser and Imaging Techniques to Fluid Mechanics, 2018, pp. 16–19.